LINEAR DRIFT WAVES IN ADVANCED STELLARATORS

A. Kendl and H. Wobig

Max-Planck-Institut für Plasmaphysik, EURATOM Association, D-85748 Garching

Drift waves are a likely cause of anomalous transport in fusion devices. The basic mechanisms of instability should be the same for both tokamaks and stellarators alike. Stabilization of drift waves, on the other hand, is mainly achieved through global and local shear damping, and by effective localization of modes through toroidicity and helical ripple wells. These stabilizing effects can differ for specific geometries, and it is in principle possible to optimize a stellarator in this respect.

Although the theory should be a direct expansion of tokamak studies, investigations in the past were sparse and adresses only a few specific geometries for helical symmetry [1,2], a torsatron [3] and heliac [4,5]. The essential questions, if in respect to the reduction of growth rates one stellarator geometry has to be favoured over an other or if an effective optimization is possible have not been addressed yet. In this contribution, we discuss in a basic electrostatic WKB model the effect of stellarator optimization due to reduction of Pfirsch-Schlüter currents on linear drift instability. The helical advanced stellarator (Helias) concept [6] is underlaid for the investigation of drift mode properties in three devices with increasing optimization: Wendelstein 7-AS, which is in operation and where experimental data are available; Wendelstein 7-X, which is under construction; and HSR, a concept study for a stellarator reactor [7]. In the table below, specific dimensions of the devices are compared. However, by using dimensionless and scale-independent formalism, focus in our study is set on geometrical aspects of optimization only.

Wendelstein 7-AS	R_0=2.1 m	a_0=0.20 m	B_0=2.5 T	T_0=1.5 keV	rot. trans. $1/4 < \iota < 2/3$
Wendelstein 7-X	R_0=5.5 m	a_0=0.52 m	B_0=3.0 T	T_0=5.0 keV	rot. transf. $5/6 < \iota < 1$
Helias Reactor	R_0=22.0 m	a_0=1.8 m	B_0=5.0 T	T_0=15.0 keV	rot. transf. $5/6 < \iota < 1$

1. Drift wave model and numerical eigenvalue code

We adopt the electrostatic drift wave model in the approximation for fluid ions and nearly adiabatic electrons. The derivation is standard: Ion continuity, momentum and quasi-neutrality equations form a closed system. From momentum balance we obtain velocities $\mathbf{v}_{\|i}$ and $\mathbf{v}_{\perp i}$, with $E \times B$ drift $\mathbf{v}_E$, ion polarization drift $\mathbf{v}_{pi}$ and ion diamagnetic drift $\mathbf{v}_{Di}$. Non-adiabaticity is retained by $\xi = 1 - i\delta$ ($\delta > 0$). Inserting into the equation of continuity, carrying out gradients and applying the usual drift ordering we obtain a second order differential equation for the perturbed electrostatic potential $\hat{\Phi} \equiv e\Phi/T_{e0}$:

$$\hat{\nabla}_{\|}^2 \hat{\Phi} = \left(\hat{U} + i\hat{V}\right) \hat{\Phi}. \quad (1) \quad \text{with}$$

$$\hat{U} = u_0\hat{\omega}\left[\hat{\omega}\left(\frac{\hat{B}\xi}{r\hat{T}_e} + rm^2|\hat{\nabla}\alpha|^2\right) - m(\mathbf{b}\times\hat{\nabla}\alpha)\cdot\hat{\boldsymbol{\kappa}}_s\right],\ \hat{V} = \frac{u_0\hat{\omega}\xi}{\hat{B}}(2\tau+\eta_i)(\mathbf{b}\times\hat{\boldsymbol{\kappa}}_B)\cdot\hat{\boldsymbol{\kappa}}_n.$$

An eikonal form is used for $\hat{\Phi} = \hat{\Phi}(\zeta)\cdot\exp(-i\omega t + im\alpha)$, where m is the (large) mode number, α=θ-$\iota\zeta$ is a function of poloidal angle θ and toroidal angle ζ in Boozer coordinates. Above, $\mathbf{b} = \mathbf{B}/B$, $\tau \equiv T_i/T_e$, $\hat{\nabla} = a_0\nabla$ and $u_0 = -4r\hat{B}\hat{J}^2/(1+\xi\tau)$. $\hat{\boldsymbol{\kappa}}_n \equiv \hat{\nabla}\ln n_0$ and $\hat{\boldsymbol{\kappa}}_B \equiv \hat{\nabla}\ln B$, and $\hat{\boldsymbol{\kappa}}_s \equiv [1+\xi\tau(\eta_i-1)]\hat{\boldsymbol{\kappa}}_n - [1+\xi\tau]\hat{\boldsymbol{\kappa}}_B$, where $\eta_i = \partial\ln T_i/\partial\ln n_0$. We denote $\hat{T}_e \equiv T_e/T_{e0}$, $\hat{B} \equiv B/B_0$, $\hat{\omega} \equiv \omega a_0/c_s$, $r \equiv \rho_{s0}/a_0$, $\eta_i = \partial\ln T_i/\partial\ln n_0$. Here $\hat{J} = [\hat{\nabla}s\cdot(\hat{\nabla}\Theta\times\hat{\nabla}\zeta)]^{-1}$ is the Jacobian, $\rho_{i0} = \sqrt{MT_{i0}}/(eB_0)$ is ion gyro radius and $c_{i0} = \sqrt{T_{i0}/M}$ is ion thermal velocity on axis. $L_n = (\partial_s\ln n_0)^{-1}$, $\hat{\xi} \equiv 1+\xi\tau(\eta_i-1)$ and $\hat{\tau} \equiv 1+\xi\tau$. For $\tau = 0$ and $\hat{T}_e = 1$, $\hat{U}$ reduces to the form used in Refs. [1,2,3,8]. By using metric elements $g^{\mu\nu} = \nabla\mu\cdot\nabla\nu$ we can express $\hat{U}$ and $\hat{V}$ as functions of geometrical values ($g^{\mu\nu}$, ι, $\nabla\ln\hat{B}$) [9]. Local shear $S = (\mathbf{b}\cdot\nabla)\sigma$ is determined by $\sigma = (g^{s\theta} - \iota g^{s\zeta} - \zeta\partial_s\iota g^{ss})/g^{ss}$.

Metrical quantities are calculated using three-dimensional numerical equilibrium code data in Fourier representation. The system of equations is solved using standard shooting techniques in a complex eigenvalue code suitably developed for three-dimensional equilibria. Only the more unstable symmetric eigenfunctions are searched for by a Mueller algorithm. For details see Refs. [2,9].

2. Linear spectrum in "$i\delta$"-approach

By solving Eq. (1) for a given equilibrium we obtain the eigenfunctions and a spectrum of eigenvalues (ω_R, γ). As matching point ζ_0=0.5, θ_0=0, s=1/4 is taken, which is a symmetry point and corresponds to a helical potential function well. Density depends as $n = n_0(1-s)^2$. For non-adiabaticity we assume an arbitrary fixed value of $\delta = 0.01$ (as e.g. in [2]). For $\delta = 0$ and $\tau = 0$ all solutions are marginally stable. Various scenarios on the effects of finite δ and τ are depicted in Fig. (1a).

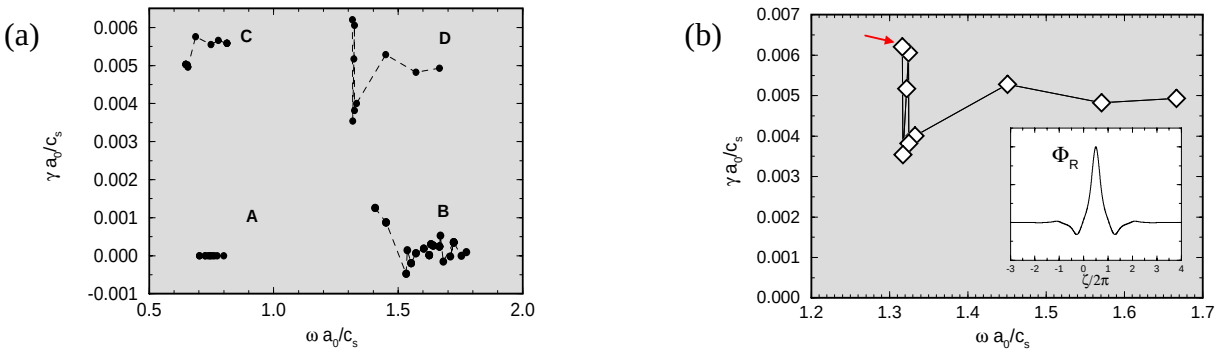

Fig. 1: a) A: τ=0, δ=0; B: τ=1, δ=0; C: τ=0, δ=0.01; D: τ=1, δ=0.01. All for W7-X with m=50, η_i=2.
b) Case D in detail with inset real wave function $\Phi_R(\zeta)$ for most unstable mode.

In accordance with Refs. [1,2,3] we find in Fig. (1b) both weakly and strongly localized modes. Mode number spectra of each of the three Helias configurations are compared in Fig. (2a). Here $r \equiv r_{W7X} = 0.005$ is set identically for all configurations.

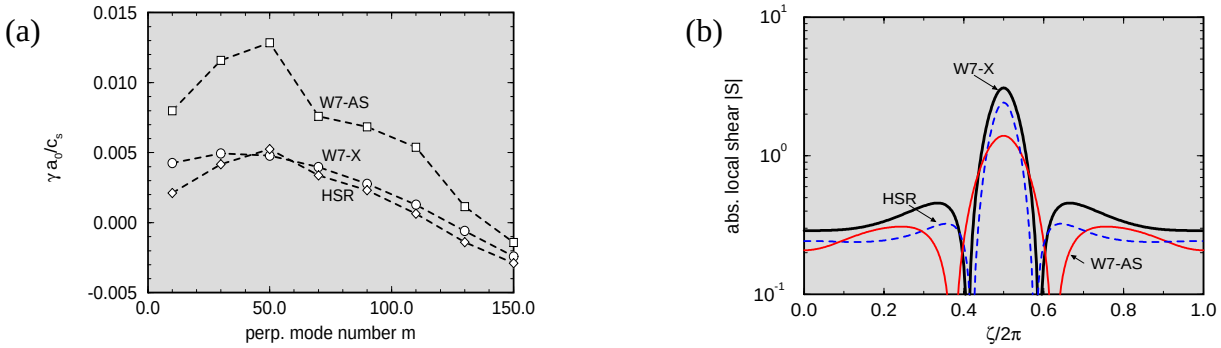

Fig. 2: a) Mode number spectra for Helias configurations W7-AS, W7-X and HSR.
b) Local shear $|S|$ in one field period on s=1/2.

The increase of $|S|$ (Fig. 2b) can be expected to have the major contribution to the observed favourable behaviour of one configuration over an other [8]. An increase of S is only an indirect consequence of optimization: In the Helias approach to reduction of Pfirsch-Schlüter currents, helicity and field line torsion are increased. Over change of pitch angle of field lines with radius, torsion again is related to shear S. Still, HSR in Fig. (2a) shows better performance for most mode numbers m despite less absolute local shear than W7-X. The seemingly dominant competing mechanism in the present warm ion model is the mostly favourable normal curvature for HSR compared to W7-X.

3. Dissipative trapped electron mode (DTEM)

Particles confined in a magnetic mirror can be detrapped by collissions, which is the cause for the trapped-particle instability. We basically follow the linear DTEM theory as treated explicitly by Dominguez *et al.* [3]. In order to focus on particle trapping effects, we restrict to $\tau = 0$. This enables the perturbative approach by arriving at a single ordinary differential equation, $\partial_\zeta^2 \hat{\Phi} = (\hat{U}_0 + \hat{U}_1)\hat{\Phi}$. Here $\hat{U}_0$ is real, and $\hat{U}_1$ is the complex perturbed potential that stems from δ, which in return is calculated from trapped electron response. For details, see Refs. [3,9]. For $\hat{U}_1 = -i\delta\hat{\omega}_0^2/\hat{T}_e$ with $\delta = \frac{2}{\sqrt{\pi}} \cdot \frac{\hat{\omega}_*}{\hat{\nu}_f} \left[\left(1 - \frac{\hat{\omega}_0}{\hat{\omega}_*}\right) + \frac{3}{2}\eta_e\right] \cdot \int \mathrm{d}\Lambda \hat{B}/(\Lambda^{3/2}\sqrt{\Lambda - \hat{B}})$, we obtain the complex change in the eigenfrequency through the perturbational calculation to be $i\gamma = -\left(\int \mathrm{d}\eta \Phi_0 U_1(\omega_0) \langle\Phi_0\rangle\right) / \left(\int \mathrm{d}\eta \Phi_0^2 \, \partial U_0/\partial\omega|_{\omega_0}\right)$, where $\langle\Phi_0\rangle = (\int \mathrm{d}t_b \Phi)/(\int \mathrm{d}t_b)$ is bounce average of the electrostatic potential over the trapping region. Integration over bounce length along the field line is between turning points, and over $\Lambda = E/(\mu B_0)$ between maximum values of B along the field line in each summed up trapping interval.

To obtain the mode number spectra in Fig. (3b) for each of the three Helias devices, $\hat{\nu}_f \equiv 0.2$ and $r = r_X$ are held constant. For W7-X and $m = 50$ the frequency spectrum is shown in Fig. (3a). Now stability ordering compatible with local shear strength is found more clearly than in the corresponding Fig. (2a). In addition to the role of local shear as previously discussed, here also interplay between trapping intervalls and regions of wave localization comes to significance.

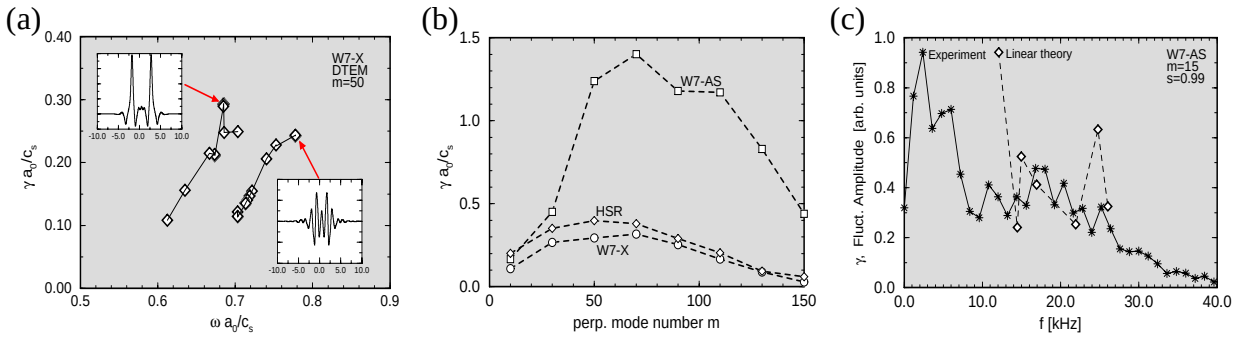

Fig. 3: a) DTEM growth rate for W7-X (m=50). Two branches can be distinguished, the first with helical localization of the wave and containing the most unstable mode, the other at larger frequencies showing toroidal localization. b) DTEM mode number spectra; c) Comparison with experiment.

4. Comparison with experiment

From linear theory only a rough mixing length estimate can be obtained for the anomalous diffusion $D \approx \gamma \Delta_r^2$, with radial mode width $\Delta_r = \rho_s/(S\Delta_\zeta)$ and average width along the field line $\Delta_\zeta^2 = (\int_{-\infty}^{\infty} d\zeta |\Phi|^2 \zeta^2)/(\int_{-\infty}^{\infty} d\zeta |\Phi|^2)$. From these and DTEM growth rates $D \approx 0.7$ m^2/s can be inferred for W7-AS, which is of realistic order.

Fluctuation data have been measured at W7-AS e.g. by Langmuir probes [10]. Spectra show qualitatively sound agreement in Fig. (3c) between experimental values and calculation for corresponding parameters. An observed feature for this boundary value of $s = 0.99$ is a highly unlocalized nature of modes ($\Delta_\zeta \approx 50$).

5. Conclusions

In this comparative numerical study of linear drift waves in Helias stellarators, a significant increase in stability has been observed for growing stellarator optimization in HSR and W7-X compared to W7-AS. This is mainly understood in terms of local shear properties. The DTE mode is able to describe qualitatively both experimentally observed diffusion and fluctuation spectrum in W7-AS. For detailed investigations, however, nonlinear mode-coupling calculations will have to be performed. Full-scale turbulence simulations are currently being prepared and will be presented elsewhere.

References

[1] A. Bhattacharjee, J.E. Sedlak, P.L. Similon et al.: Phys. Fluids **26**, 880 (1983).

[2] M. Persson, J.L.V. Lewandowski, and H. Nordman: Phys. Plasmas **3**, 3720 (1996).

[3] N. Dominguez, B.A. Carreras, V.E. Lynch, and P.H. Diamond: Phys. Fluids B **4**, 2894 (1992).

[4] J.L.V. Lewandowski: Phys. Plasmas **4**, 4023 (1997).

[5] J.L.V. Lewandowski: Plasma Phys. Control. Fusion **40**, 283 (1998).

[6] J. Nührenberg and R. Zille: Phys. Lett. A **114**, 129 (1986).

[7] H. Wobig: Plasma Phys. Control. Fusion **35**, 903 (1993).

[8] R.E. Waltz and A.H. Boozer: Phys. Fluids B **5**, 2201 (1993).

[9] A. Kendl and H. Wobig: *to be published in* Phys. Plasmas.

[10] J. Bleuel: *private communication*, 1998.